IABSE-JSCE Joint Conference on Advances in Bridge Engineering-II, August 8-10, 2010, Dhaka, Bangladesh. ISBN: 978-984-33-1893-0
Amin, Okui, Bhuiyan (eds.) www.iabse-bd.org

Finite element analysis of joint connection in steel-concrete hybrid Langer bridge

T. Maki
Saitama University, Saitama, Japan
C. Kawamura
Hokkaido Railway Company, Hokkaido, Japan
T. Ueda
Hokkaido University, Hokkaido, Japan
S. Tsuchiya
COMS Engineering Corporation, Tokyo, Japan
T. Watanabe
Hokubu Consultant Co. Ltd., Hokkaido, Japan

ABSTRACT: Steel-concrete hybrid PC Langer bridge, which consisted of RC arches, vertical steel tube hangers and PC stiffening girders, was constructed. Three dimensional numerical simulation of steel-concrete connection between the RC arch and the vertical steel tube hanger were conducted for the future establishment of verification technique of joint connection in hybrid structures using finite element method. The assembled finite element model was verified with sufficient accuracy for the mechanical behavior of the test specimens of the connection subjected to pull-out load in the steel tube. Furthermore, according to the result of numerical simulation with the partial model of joint connection in the actual bridge, it was numerically confirmed that the connection had a sufficient resistance to the pull-out load through the vertical steel tube.

1 INTRODUCTION

The steel-concrete hybrid PC Langer bridge, which consisted of reinforced concrete (RC) arches, vertical steel tube hangers and prestressed concrete (PC) stiffening girders as shown in Figure 1, was constructed in Hokkaido, Japan. Many existing Langer bridges were constructed using single material such as steel or concrete, and no other examples of similar type of structures to the current target bridge exist. Three-dimensional frame analysis was conducted in the design, in which train load was applied as a moving load to the frame model of the bridge, and the component members of the bridge were designed for the computed sectional forces. Much attention was paid to the design of joint connection between steel tube hanger and RC arch, of which resistance to the pull-out force through the hanger to the arch was dominant in the design. Loading tests of model specimens of joint connection were also conducted to verify the design result.

The structural performance verification of the bridge was made according to the design standard for railway structures (RTRI 2007). Standard Specifications for Hybrid Structures was also published by the Japan Society of Civil Engineers (JSCE 2009), which describes an integrated performance verification method using finite element analysis (FEA) and nonlinear material constitutive laws. However, there are still few examples of verification of special joint connection design. Based on such background, three-dimensional FEA was conducted for loading test of model specimen and finite element modeling concept was verified. Furthermore, numerical investigations were also conducted on the influences of span length of RC arch on the mechanical behavior and failure pattern of the joint connection.

Figure 1. Steel-concrete hybrid PC Langer bridge

2 DETAIL OF JOINT CONNECTION IN LANGER BRIDGE AND TEST SPECIMENS

2.1 *Profile of the target bridge and its joint connection*

The target Langer bridge, having 65m span length, consists of two RC arches and PC stiffening girders connected each other with fourteen steel tube hangers. Span-to-rise ratio is 1/5.8 and the rise is about 9.6m. The overall configuration of the bridge is shown in Figure 2. The detail of the arch member and the center joint connection are shown in Figure 3. The longitudinal and lateral reinforcing bars in the arch and the main bars in the strut are penetrated through the steel tube embedded into the arch. The bearing (anchor) plates and the stiffeners are also provided at the end of the steel tube. SM490YB (JIS) plate having 16mm thickness is used for the steel tube, and SM400A (JIS) plate with 20mm thickness is adopted for both the anchor plates and the stiffeners. In the RC arches and struts, SD345-D32 (JIS) and SD345-D16 (JIS) deformed bars are provided as longitudinal and lateral reinforcement. The longitudinal bars in the strut are anchored to the concrete inside the steel tube in the joint connection by the 80mm anchor plates welded at the end of the bars. Design strength of concrete is 60N/mm^2 for arches and 40N/mm^2 for struts. Concerning the design of joint connection at the center of the bridge, the design pull-out force in the steel tube hanger and the design axial force in the RC arch are 949.7kN and 7477.3kN, respectively.

The behavior of a bridge structure under the influence of seismic load has been a major point of interest for engineers over a long period of time. Although significant advances have been achieved in the design and construction of an earthquake resistant bridge, numerous gaps still remain in the understanding of the seismic behavior of bridges. The objective of the present research is to analyze the longitudinal and transverse earthquake motion of the bridge and to determine the design forces and moments at the column bases following the equivalent static force method and response spectrum method. Then a comparative study of the design forces and moments found from these two cases has been performed. It is expected that the findings of this study will lead to a better understanding of the behavior of bridge under seismic loading. For simplicity of the analysis, linear material behavior and fixed support conditions are assumed in this study.

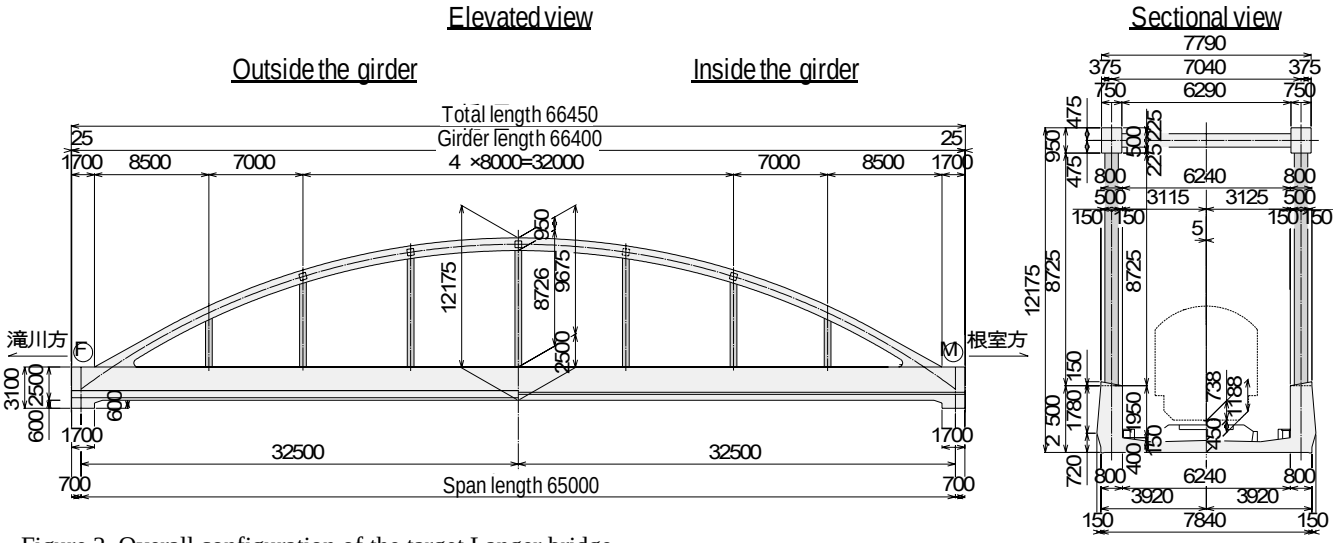

Figure 2. Overall configuration of the target Langer bridge

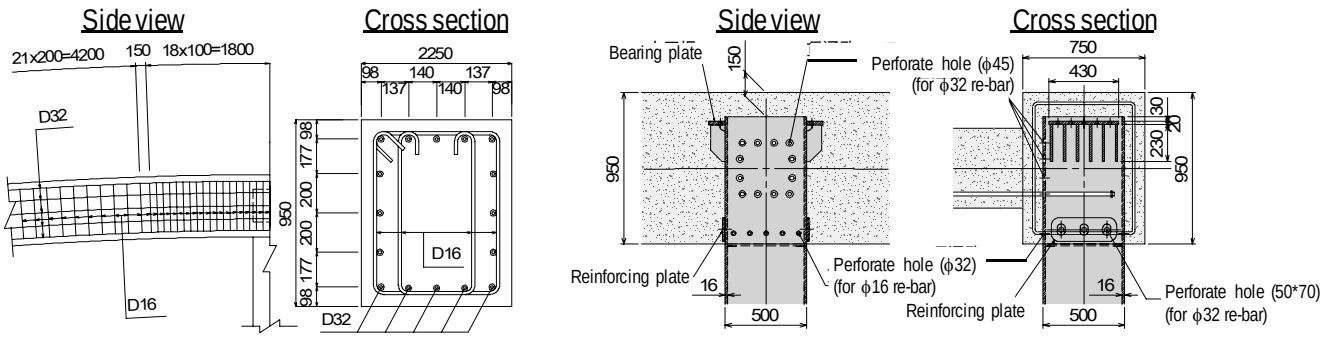

Figure 3. Detail of center joint connection

2.2 *Test specimens*

The loading tests of joint connection specimens were conducted in order to verify the damage level of the connection under design load (Kawamura et al. 2007, Doi et al. 2009). The capacity of joint connection against pull-out force through the steel tube varies with the axial force level in the arch. Therefore, the applied axial force to the arch was selected as an experimental parameter, as 0.0 (No.1), 0.19 (No.2) and 0.3 (No.3) of the axial force ratios defined as a ratio of the applied axial force to the ultimate axial force of the arch, in consideration of the design axial force ratio of 0.19 in the actual bridge. As shown in Figure 4, the specimen with a span length of 2.2m, in which a shear span-to-depth ratio was lower than the actual bridge, was designed to fail in shear in the arch, instead of the failure of connection itself. The comparisons of design details of the actual bridge and the specimen are summarized in Table 1. The target of the specimen was the center connection in the bridge because the pull-out shear force in the arch was a critical parameter at the center compared to the other connections in the design. The compressive strength of concrete was 64.9 to 68.5N/mm^2 for three specimens, and the yield strength and Young's modulus of reinforcing bars were 430N/mm^2 and 196kN/mm^2 for D19 bars, and 432N/mm^2 and 197kN/mm^2 for D10 bars, respectively. The left stub was fixed to the floor by PC tendons, whereas the right stub was rigidly fixed to the floor during the loading. Pull-out load was applied to the top end of steel tube under constant axial load to the left stub of the specimen. DAH-1 to 5 in Figure 4 indicate the numbers of displacement transducers.

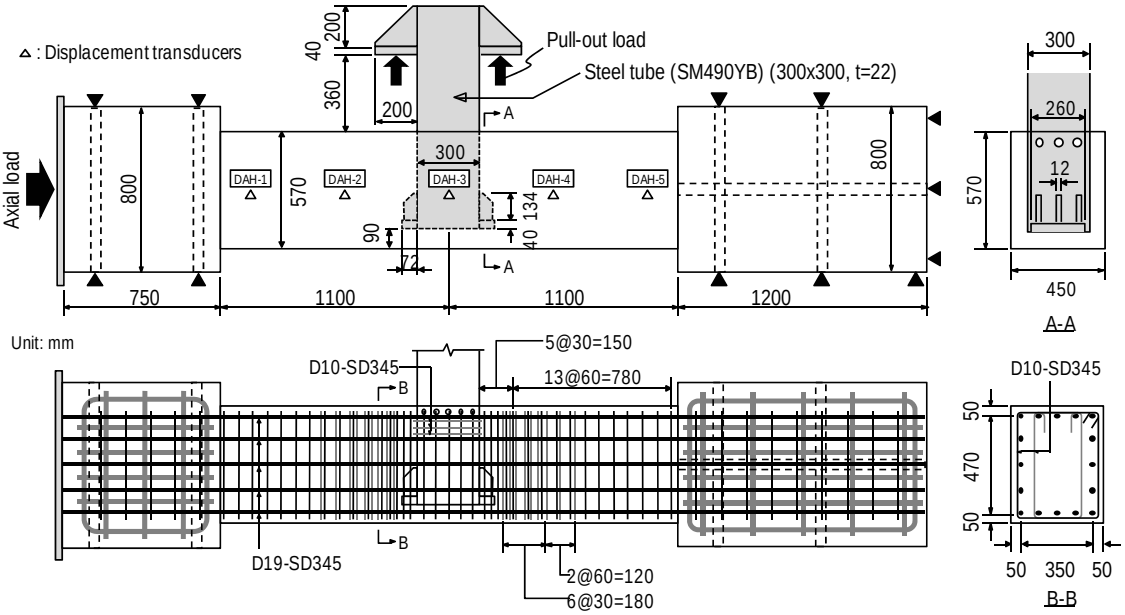

Figure 4. Dimensions and reinforcement arrangement of test specimen

Table 1. Comparisons of design details between the actual bridge connection and the specimen

			Actual bridge	Test specimen
Cross section	Width	b (mm)	750	450
	Effective depth	d (mm)	852	520
	Section height	h (mm)	950	570
Longitudinal reinforcement	Arrangement	*Nos.- Dia.*	16-D32	16-D19
	Area	A_p (mm^2)	12672	4560
	Ratio	p (%)	1.78	1.78
Lateral reinforcement	Arrangement	*Dia.@ spacing*	D16@100mm	D10@60mm
	Area	A_{pw} (mm^2)	3960	1425
	Ratio	p_w (%)	0.62	0.61

2.3 *Summary of test result*

Figure 5 shows the crack diagrams of the specimens after loading. All the specimens failed in shear in the right span, due to the asymmetric fixity of the left and right stubs in the test. The angle of critical diagonal crack lowered with an increase of axial load level.

Figure 6 shows the relationships between the applied pull-out load and the arch displacement of the specimens. The maximum capacity was higher in the specimen under higher axial load level, as similar to the tendency observed in the ordinary RC members. The longitudinal reinforcements in all the specimens were yielded in tension only at a location just close to the steel tube, due to the influence of relative displacement of the tube to RC arch. Some of the lateral reinforcements were also yielded at the intersections of the bars and the critical diagonal crack that led to the diagonal shear failure in the shear span of the specimens.

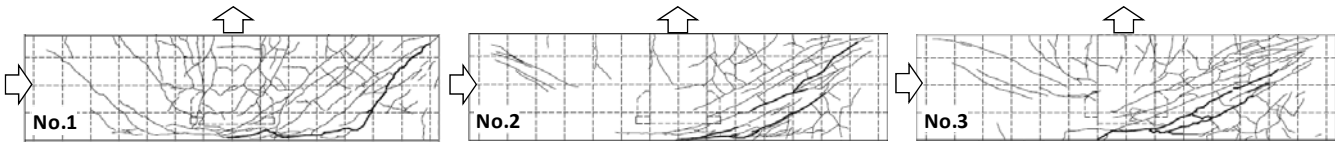

Figure 5. Crack diagrams after loading

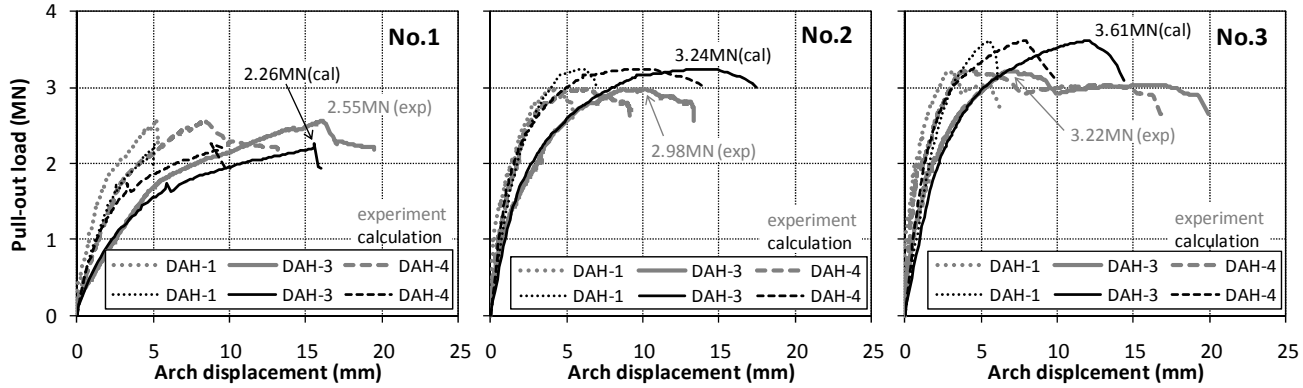

Figure 6. Relationships between pull-out load and arch displacement

3 NUMERICAL SIMULATION OF TEST SPECIMENS USING FINITE ELEMENT ANALYSIS

3.1 *Modeling of test specimens*

Numerical simulations of the specimens tested in the previous section were conducted using the three-dimensional nonlinear finite element analysis program COM3 (Okamura et al. 1991, Maekawa et al. 2003), developed in the University of Tokyo, Japan. The finite element mesh used in the simulations is shown in Figure 7. The half of the specimen was modeled in consideration of the symmetry of the problem, and three-dimensional 20-node solid (brick) elements were used for both RC and steel parts.

The existing example of FEA to the hybrid structures (Hauke et al. 1999) was referred in the assembling of the model, based accurately on the reinforcement arrangement in the specimen. The effective zone of bond between concrete and deformed bar (An et al. 1997), as well as the element size in relation to the control volume of the applied constitutive laws (JSCE 1997), was carefully considered. The localized deformation of

penetrated reinforcing bars through the perforated holes on the steel tube was considered by providing RC joint elements (Okamura et al. 1991) at the exact location between steel and concrete elements, and no shear slip resistance was assumed at the other portion of the steel tube surface.

The boundary conditions in the both stubs were adjusted to the test condition; i.e. the right stub was rigidly fixed whereas the left stub was fixed by two truss elements in which 5000 of initial prestressing strain was introduced.

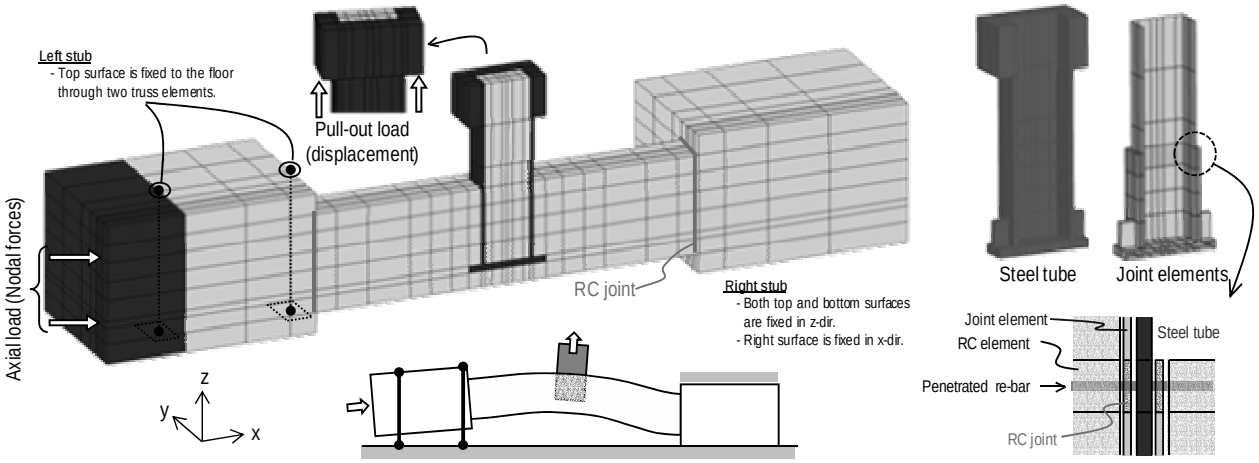

Figure 7. Finite element model used in the simulation of pull-out test

3.2 *Material constitutive laws and parameters*

The nonlinear path-dependent constitutive law of reinforced concrete, proposed by Okamura and Maekawa (Okamura et al. 1991), was applied to the RC elements in the arch part. The applied model consists of multi-directional compression-tension-shear model of concrete and reinforcement, with non-orthogonal four-way fixed crack model based on the smeared crack assumption, and it has already been verified for nonlinear behavior of RC structures under various types and combinations of external loads as well as the seismic excitations. The values of material parameters shown in the previous section were used as input parameters to the constitutive laws. The post-peak relation in the stress-strain curve of concrete in the non-effective zone of bond with reinforcement was carefully defined in consideration of fracture energy of the material (An et al. 1997, El-Kashif et al. 2004, Nakamura et al. 2001). Note that such attention shall be paid in the modeling of steel-concrete hybrid structures because the element size highly depends not only on the reinforcement arrangement but also the dimensions of steel members and elements.

3.3 *Result of numerical simulations*

The relationships between pull-out load and displacement obtained by the numerical analysis are shown in Figure 6 together with the test results. Although the maximum pull-out load in No.2 and No.3 are slightly overestimated, numerical result of the deflection at the center of the specimen, as well as that at the point in the shear span, has a good agreement with the test results. In the vertical strain contour plots of the specimens at their maximum loads, shown in Figure 8, high strains with inclined distribution are observed in the right span rather than in the left span, as similar to the crack diagrams shown in Figure 5. Therefore, it is concluded that the proposed FE model can predict the damage and failure of the target joint connection due to the pull-out load in the steel tube.

3.4 *Influence of shear span length on the behavior of joint connection*

The joint connection in the actual bridge is designed such that flexural damage in the arch precedes the failure of the connection itself when the steel tube is subjected to vertical pull-out force. However, the actual sectional forces in the component members of the bridge depend on the loading condition, resulting in the variation of the ratio of pull-out force in the steel tube to the bending moment in the arch.

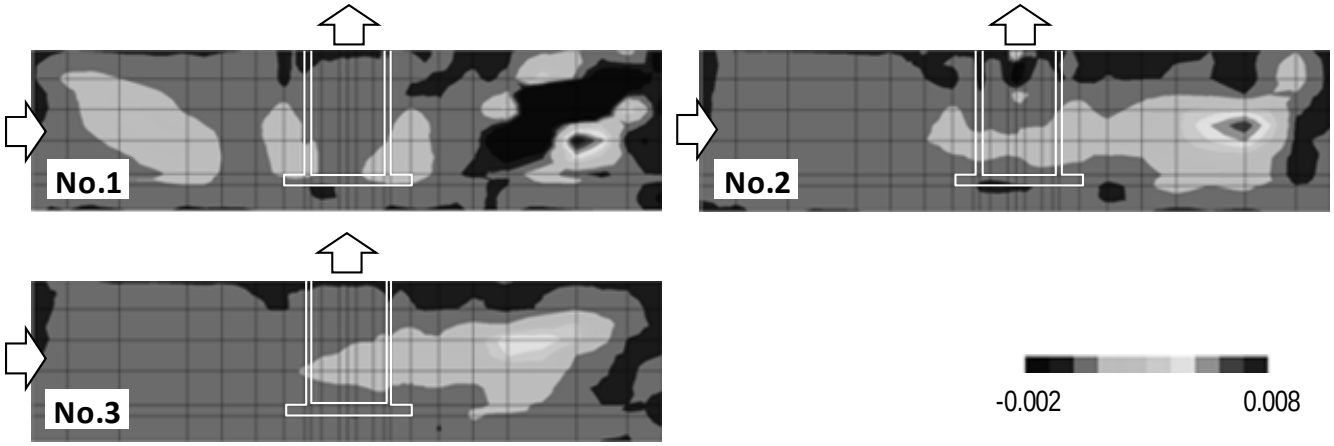

Figure 8. Vertical strain contour plots of the specimens

Therefore, from the view point of critical design of the bridge, the importance to grasp the critical capacity of the connection itself can be emphasized. Based on the background, the parametrical numerical analysis was conducted on the influence of shear span length of arch on the joint capacity and the failure pattern of the arch. The assembled FE model is shown in Figure 9. The mesh divisions of the embedded portion of the steel tube and of the arch member were completely coincide with those in the model shown in Figure 7, whereas the arch member was simply supported with the support plates having 12cm width. The axial force equivalent to the axial force ratio of 0.19 was applied at the both ends of the arch, and the top end of the steel tube was subjected to the pull-out load. Note that the nominal shear span length *a* here was defined as the horizontal distance from the edge of the anchor plate in the connection part to the support, and the effective depth *d* was defined as the vertical distance from the edge of the anchor plate to the top end of the arch member (*d* = 44cm). The location of the support plate was varied horizontally to change the nominal shear span length from 15.8 to 185.3cm, resulting in the variation of nominal shear span-to-effective depth ratio *a/d* from 0.359 to 4.211.

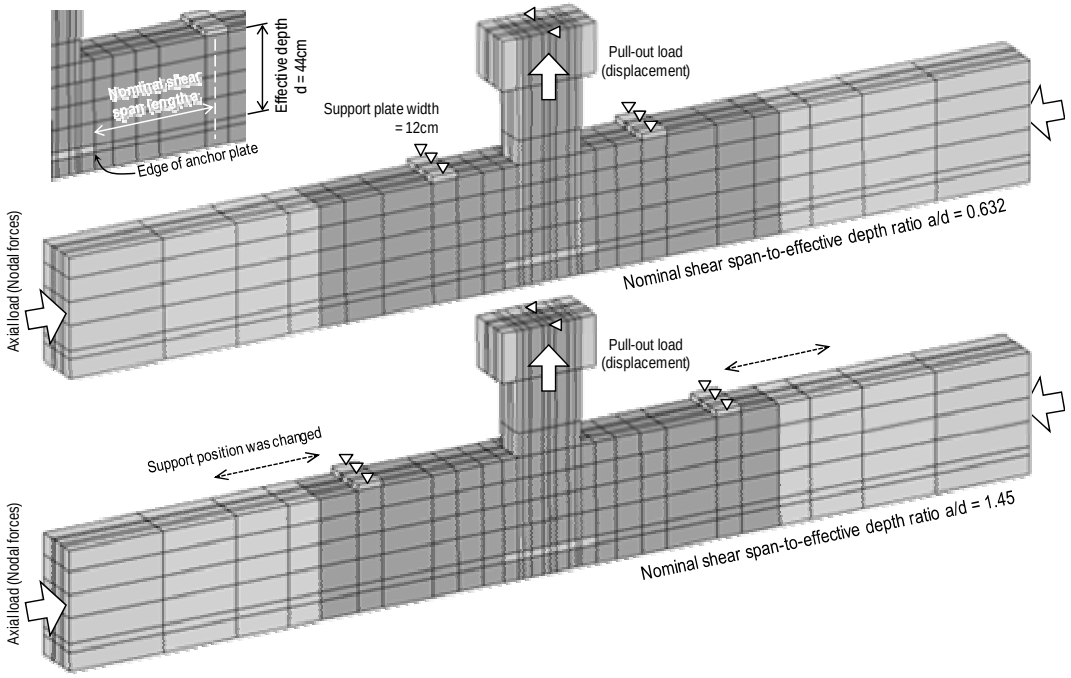

Figure 9. Finite element model used in the parametric investigation

Figure 10 shows the relationships between the applied pull-out load and the vertical displacement at the loading point and the variation of the maximum pull-out load with the different values of nominal shear span-to-depth ratio. The calculated pull-out loads P_{mu} equivalent to the ultimate bending moment obtained by the sectional analysis of arch member are also shown on the right in Figure 10. According to the obtained load-displacement curves, the ductile behavior was exhibited in the case with large *a/d* ratio although the lower

maximum pull-out load was obtained, whereas in the case with low *a/d* ratio the brittle behavior was observed where the remarkable decrease in the pull-out load after the maximum load was reached. Furthermore, in the cases with *a/d* ratio higher than 1.0, the maximum pull-out load coincided with P_{mu} indicated that the maximum load was governed by the flexural failure of the arch. On the contrary, the maximum pull-out load was lower than P_{mu} in the cases with *a/d* ratio lower than 1.0, resulting in the occurrence of failure prior to the ultimate flexural failure. The contour plots of longitudinal strain and shear strain at the maximum pull-out load in the cases with *a/d* = 0.632 and 1.859, as examples, are shown in Figure 11. Here, deformation of each element is magnified by five times as large as the original deformation. As indicated, flexural failure occurred in the case with *a/d* = 1.859 because a very high compressive strain could be observed in the concrete beneath the steel tube together with a high tensile strain in the tensile concrete just beside the steel tube. However, in the case with *a/d* = 0.632, the tensile strain in the upper end of the arch was not remarkable and a high shear strain distributed from the edge of the anchor plate to the top end of the arch. In addition, the opening gap could be observed between the bottom end of the steel tube and the concrete beneath the tube in this case. Therefore, the pull-out failure of the connection itself preceded the flexural failure of the arch in the cases with low *a/d* ratio, although the maximum pull-out load itself might be influenced by the width of the support plates. According to the results, it can be concluded, at least, that the ductile flexural failure in the arch would be reached at the ultimate state with the nominal shear span-to-depth ratio higher than 1.0.

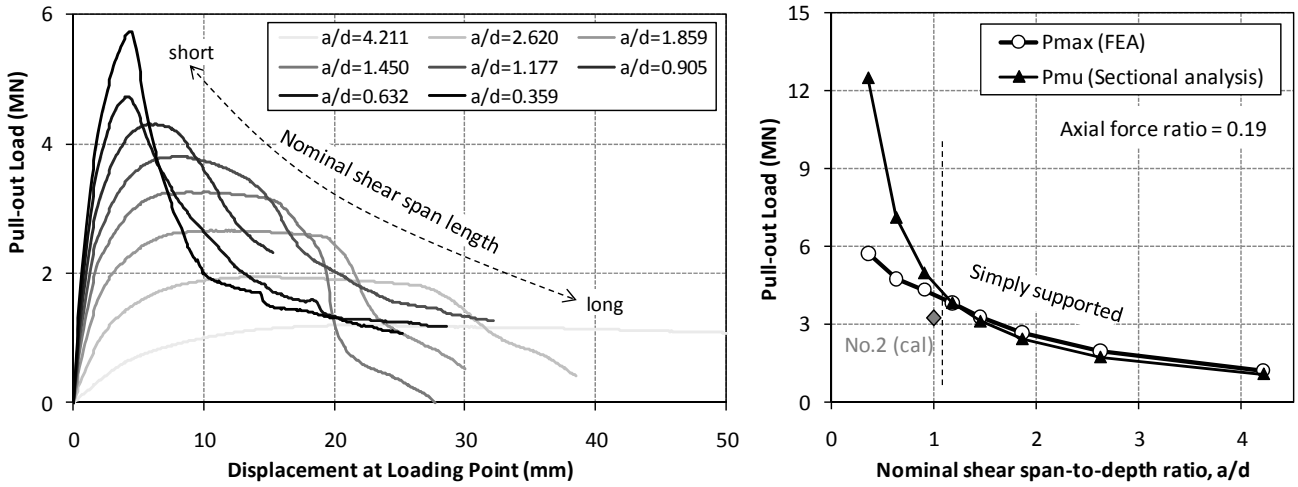

Figure 10. Influence of nominal shear span-to-effective depth ratio on the mechanical behavior of joint connection

4 NUMERICAL SIMULATION OF JOINT CONNECTION IN ACTUAL BRIDGE

4.1 *Modeling*

The numerical simulation of the pull-out behavior of center joint connection in the actual bridge shown in Figure 2 was conducted with the FE model assembled with the same modeling policy stated in the previous section. According to the bending moment distribution diagram obtained by the preliminary frame analysis, the total span length of the arch in the partial model, as shown in Figure 12, was determined as 5m, and the both ends of the arch were simply supported at the mid height on the end surface. The effective depth in the joint connection was 751mm, given as the distance between the edge of the anchor plate and the bottom end of the arch. Consequently, the nominal shear span-to-depth ratio was 2.863. The actual arch member had a curved shape with 54m radius at its mid height; however, the arch was modeled as a straight member because the span length was not so long.

Only the pull-out load was applied to the vertical steel tube because the bending moment and shear force in the steel tube under the design load were negligible. Because the Langer bridge is a statically-indeterminate structure, the sectional forces in the component members depend on the deformation level of the bridge. Especially, both the pull-out force in the steel tube and the axial force level in the arch are dependent on the applied load on the bridge deck. In order to consider this fact, the incremental pull-out load was applied to the steel tube, with the ratio of the applied axial load to the pull-out load kept constant as 7.87, given as the ratio of design sectional forces (N_d/P_d = 7.48 / 0.95 = 7.87, where, N_d and P_d are design axial force and design pull-out force, respectively.).

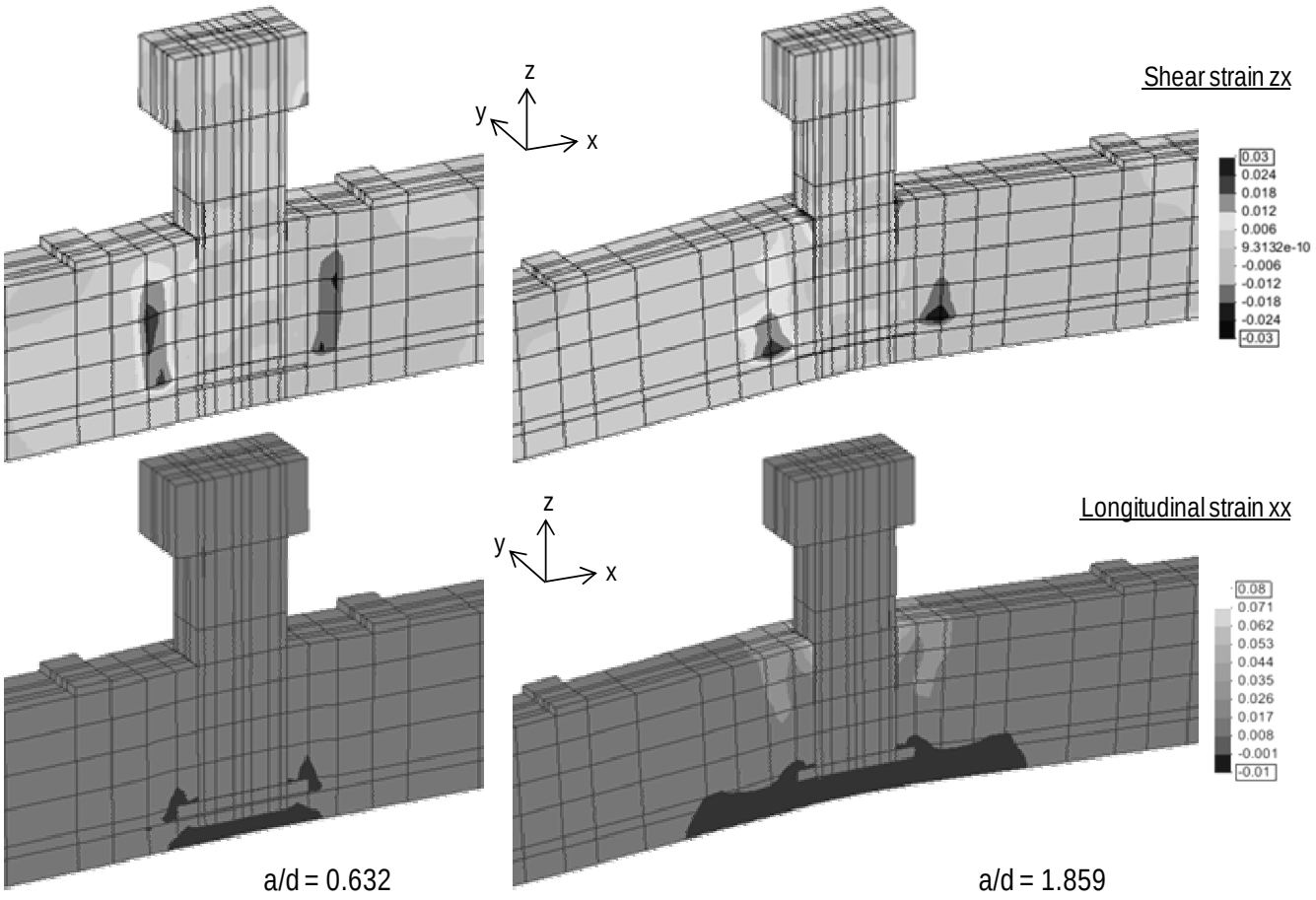

Figure 11. Deformations and strain contour plots of the cases with a/d = 0.632 and 1.859

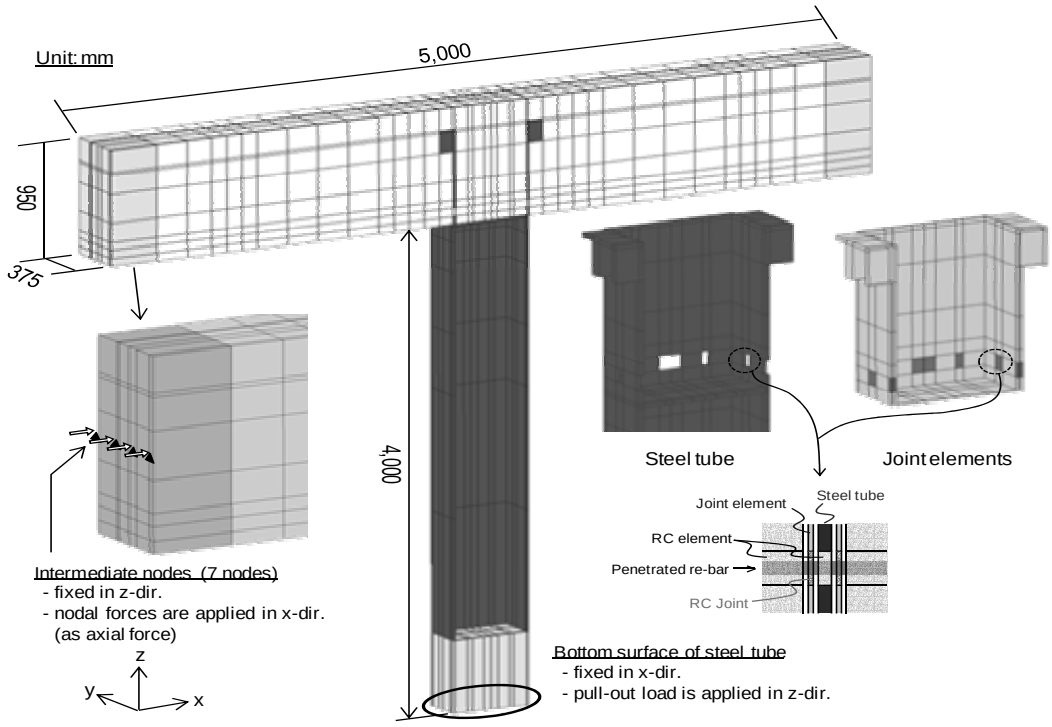

Figure 12. Finite element model used in the simulation of joint connection in the actual bridge

4.2 *Result of simulation*

The overall deformation and the longitudinal strain contour plot are shown in Figure 13. Here, deformation is magnified by 10 times as large as the original deformation. No relative displacement of the steel tube to the arch (pull-out displacement) could be observed even at the maximum pull-out load (about 4 times as large as the design pull-out load), and the bottom end of the arch still remained in compression due to the high axial force in the arch. Because the localized high compressive strain occurred at the top end of the arch just above the steel tube, the ultimate state of the joint connection was governed by the flexural compression failure of the arch. Figure 14 shows the pull-out load and displacement relation and the interaction curve of the arch section. P_{mu} is the calculated pull-out load equivalent to the ultimate bending moment of the arch section under the maximum axial force N'_{max} equal to $7.87P_{max}$. In the interaction curve, the bending moment was converted to the pull-out load through the shear span length. The fact that the maximum pull-out load in the simulation was reached P_{mu} proved the sufficient capacity in the joint so that it can transfer the pull-out force in the steel tube to the arch as bending moment. Furthermore, it was confirmed that the joint had a sufficient safety capacity against the design sectional forces used in the verification of the ultimate limit state in the practical design process.

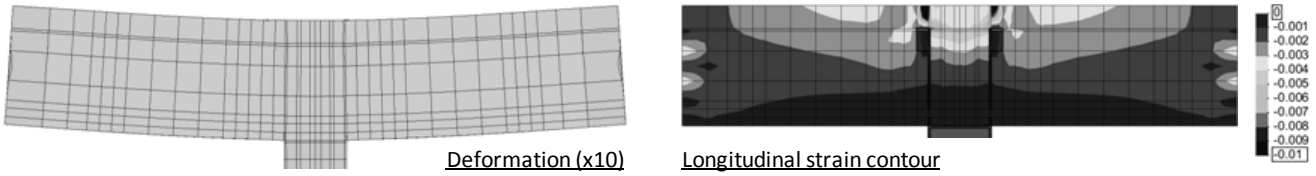

Figure 13. Deformation and longitudinal strain contour plot when the maximum load was reached

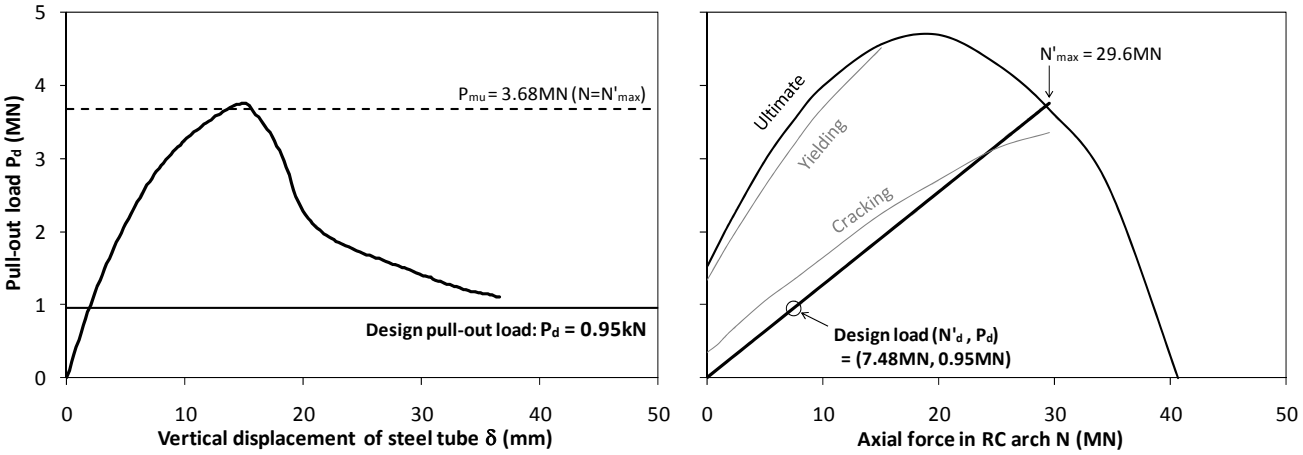

Figure 14. Relationship between pull-out load and displacement at loading point and the interaction curve of arch section

5 CONCLUSIONS

Numerical simulations using three-dimensional finite element method were conducted on the pull-out loading test specimens and the joint connection in the actually-constructed steel-concrete hybrid Langer bridge. The conclusions are summarized as follows:

(1) The assembled finite element model was verified for the pull-out loading test specimens under different axial loads, which gave the simulated result having a good agreement with the test results.
(2) The parametrical investigations on the influence of shear span-to-depth ratio on the damage and failure pattern of the joint connection were also conducted. Within the range of the parameters in this study, it was clarified that the joint with the nominal shear span-to-depth ratio over 1.0 exhibits the ductile flexural failure in the arch under the constant axial load.
(3) Based on the proposed modeling policy, the pull-out simulation of the joint connection in the actual hybrid Langer bridge was conducted under the incremental axial load to the arch member. It was confirmed that the designed joint connection had a sufficient capacity to transfer the pull-out force in the steel tube hanger to the arch as bending moment.

ACKNOWLEDGEMENT

The finite element analysis code was offered by Professor Koichi Maekawa in the University of Tokyo. His kind cooperation and support are gratefully acknowledged.

REFERENCES

An, X., Maekawa, K. & Okamura, H. 1997. Numerical simulation of size effect in shear strength of RC beams, *Journal of Materials, Concrete Structures and Pavements*: No.564/V-35, 297-316. Tokyo: JSCE.

Doi, S., Kawamura, C., Edamatsu, M. & Matsuoka, S. 2009. A study on the safety of the RC-steel joint of composite PC Langer bridge with through girder, In JCI (eds), *Proceedings of the Japan Concrete Institute*: Vol.31, 1183-1188. Tokyo: Japan Concrete Institute. (in Japanese)

El-Kashif, F.K. & Maekawa, K. 2004. Time-dependent nonlinearity of compression softening in concrete. *Journal of Advanced Concrete Technology*: Vol.2, 233-247. Tokyo: Japan Concrete Institute.

Hauke, B. & Maekawa, K. 1999. 3D FEM tool for performance evaluation strengthened RC members. *Journal of Materials, Concrete Structures and Pavements*: No.634/V-45, 369-386. Tokyo: JSCE.

Japan Society of Civil Engineers 1997. *Final Report of Subcommittee on Constitutive Models (301)*, Concrete Gijutsu Series 21. Tokyo: JSCE. (in Japanese)

Japan Society of Civil Engineers 2009. *Standard Specifications for Hybrid Structures*. Tokyo: JSCE. (in Japanese)

Kawamura, C., Watanabe, T., Matsuoka, S. & Edamatsu M. 2007. Design of Joint Connection in Hybrid PC Langer Bridge. In JSCE (eds), *The 7th Symposium on Application of Hybrid Structures*: 17-1-6. Tokyo: JSCE. (in Japanese)

Maekawa, K., Pimanmas, A. & Okamura, H. 2003. *Nonlinear Mechanics of Reinforced Concrete*. London: Spon Press.

Nakamura, H. and Higai, T. 2001. Compressive fracture energy and fracture zone length of concrete. In Shing, P. B. & Tanabe, T. (eds), *Modeling of Inelastic Behavior of RC Structures under Seismic Loads*: 471-487. ASCE.

Okamura, H. & Mekawa, K. 1991. *Nonlinear Analysis and Constitutive Models of Reinforced Concrete*. Tokyo: Gihodo Shuppan.

Railway Technical Research Institute 2007. *Design Standard for Railway Structures – Steel-Concrete Hybrid Structures*. Tokyo: Maruzen. (in Japanese)